Matched phase sweep method for the optimization of bunching factor in dual rf systems of high-intensity hadron synchrotrons

H. Y. Liu,[1,2,3,*] Y. S. Yuan,[1,2,3,*] S. Y. Xu,[1,2,3] L. S. Huang,[1,2,3] X. H. Lu,[1,2,3] and S. Wang[1,2,3,†]

[1]*Institute of High Energy Physics, Chinese Academy of Sciences, Beijing 100049, China*
[2]*University of Chinese Academy of Sciences, Beijing 100049, China*
[3]*Spallation Neutron Source Science Center, Dongguan 523803, China*

(Received 17 July 2023; accepted 8 April 2024; published 24 April 2024)

The scheme of multiturn painting beam injection in a dual harmonic rf system is widely employed in high-intensity proton or heavy ion synchrotrons to alleviate space charge effects. With a momentum offset of the injected beams, a large bunching factor can be achieved at the end of multiturn painting injection process. However, the momentum offset can increase the instantaneous beam peak current during the first 1/4 synchrotron period, causing a reduced bunching factor during the beam injection process. To address this issue, a matched phase sweep method is developed. By matching the synchrotron oscillation frequency and beam injection period, an optimal curve for phase sweeping can be directly obtained. The effectiveness of the method has been checked via simulations and machine study, which are in good agreement. The matched phase sweep method is employed for the increase of the beam power in the upcoming upgrade project of the China Spallation Neutron Source and can also be generally applied for the operation in the presence of dual harmonic rf system in high-intensity hadron synchrotrons.

DOI: 10.1103/PhysRevAccelBeams.27.044201

I. INTRODUCTION

The space charge effect is an essential limit on the beam current for high-intensity hadron (proton or heavy ion) synchrotrons, especially during beam injection [1,2]. A widely employed approach to alleviate the space charge effect is the adoption of the multiturn painting injection scheme in a dual harmonic rf system. By adjusting the ratio of the rf voltage amplitudes in the fundamental and the second harmonic rf systems, a flattened rf bucket can be obtained in which the peak beam current is reduced. Furthermore, by increasing the momentum offset of the injection beams, a large bunching factor can be achieved at the end of the multiturn painting injection process [3–7]. However, in the presence of momentum offset, the bunching factor decreases in the first one quarter of the synchrotron oscillation period during beam injection. More particles are accumulated in one-end of the rf bucket, increase the local peak beam current and the (transverse) space charge strength, and consequently deteriorate beam quality. To address this issue, a phase sweep scheme was proposed by Yamamoto *et al.* [8] to improve the bunching factor *during* the beam injection period. Specifically, in this scheme, a programmed linear sweeping of the synchronous phase of the second harmonic rf system is performed during beam injection. This scheme has been proved experimentally to be an effective way to improve the bunch shape and the bunching factor during beam injection [9].

As a high-intensity proton synchrotron, the rapid cycling synchrotron (RCS) of the recently built the China Spallation Neutron Sources (CSNS) [10,11] raises a similar issue of the space charge suppression during beam injection. Main parameters of the CSNS RCS are summarized in Table I. With a step-by-step experimental study, the designed 100 kW beam power has been successfully achieved with a tolerable beam loss level in February 2020 [12]. For the upcoming upgrade project of the CSNS RCS with the goal of 200 kW beam power (the final goal of the beam power is 500 kW with the upgrade of the CSNS linac [13]), a magnetic alloy loaded rf cavity has been recently installed in the CSNS RCS. With the combination of the ferrite-loaded rf cavities, it forms a dual harmonic rf system [14,15]. In October 2022, the beam power of the CSNS RCS has reached 140 kW with the utilization of the dual harmonic rf system.

Recently, the phase sweep method has been adopted in the beam commissioning to improve the bunching factor during beam injection in the CSNS RCS. It was shown that with this method, the bunching factor is increased. In the phase sweep method, the bunching factor optimization

*These authors contributed equally to this work.
†wangs@ihep.ac.cn

TABLE I. Main parameters of the CSNS RCS.[a]

Parameters (unit)	Value
Circumference (m)	227.92
Harmonic number	2
Repetition rate (Hz)	25
Cycling period (ms)	20
Injection kinetic energy spread (%)	±0.05
Injection fundamental rf frequency (MHz)	1.022
Extraction fundamental rf frequency (MHz)	2.444
Number of particles per bunch	$7.8 \times 10^{12}(\times 2)$
Beam power on target (kW)	100 (200)
Injection kinetic energy (GeV)	0.08
Extraction kinetic energy (GeV)	1.6
Transition gamma	4.89
Chopper duty	0.5
Horizontal painting emittance (mm mrad)	170
Vertical painting emittance (mm mrad)	155
Horizontal bare tune	4.80
Vertical bare tune	4.87

[a]The values planned for the upgrade project of the CSNS RCS are listed in the brackets.

mainly relay on numerous attempts of particle simulations. The phase sweep method for bunching factor optimization can be performed only in a qualitative manner.

In this paper, we propose a *matched* phase sweep method for bunching factor optimization, in which the phase-sweeping curve is determined by matching the synchrotron oscillation frequency to the beam injection period. The physical mechanism of the matched phase sweep scheme is quantitatively analyzed. On this theoretical basis, we show the advantage of the matched phase sweep method, and the agreement between the linear phase sweeping and the proposed matched phase sweeping for some special cases.

This article is organized as follows. After the introduction in Sec. I, the relevant longitudinal beam dynamics is briefly described in Sec. II. Section III introduces the quantitative linear phase sweep method. The matched phase sweep method is proposed, and its physical mechanism is detailed described in Sec. IV with PIC simulations. In Sec. V, as an experimental demonstration, we present the measurement results of the bunching factor with the adoption of the matched phase sweep method in the CSNS RCS. A general analysis on the advantage of the matched phase sweep scheme is elucidated in Sec. VI. Finally, conclusions are given in Sec. VII.

II. FUNDAMENTALS

The Hamiltonian for a single particle in a dual harmonic rf system is given by [16]

$$H = \frac{1}{2}\frac{h_1\eta\omega_0^2}{\beta_s^2 E_s}\left(\frac{\Delta E}{\omega_0}\right)^2 + U_1(\phi) + U_2(\phi), \tag{1}$$

in which ϕ is the phase coordinate. ΔE is the energy difference between the particle considered and the synchronous particle. ω_0 is the angular revolution frequency. β_s and E_s are the relativistic velocity factor and the energy of the synchronous particle, respectively. h_1 is the harmonic number in the fundamental rf system; η is the phase slip factor; $U_1(\phi)$ and $U_2(\phi)$ are the potential function of the fundamental and the second rf system, respectively. For the usually employed dual rf systems with sinusoidal waveform, we have

$$U_1(\phi) = \frac{eV_1}{2\pi}[(\cos\phi - \cos\phi_{1s}) + (\phi - \phi_{1s})\sin\phi_{1s}], \tag{2}$$

and

$$U_2(\phi) = \frac{-eV_2}{2\pi h_r}[\cos(\phi_{2s} + h_r(\phi - \phi_{1s})) - \cos\phi_{2s} - h_r(\phi_{1s} - \phi)\sin\phi_{2s}]. \tag{3}$$

Here e is the unit of charge. V_1, V_2 and ϕ_{1s}, ϕ_{2s} are, respectively, the rf voltage amplitudes and the synchronous phases in the fundamental rf system and in the second rf system, with $\phi_{2s} = \phi_2 + h_r\phi_{1s}$ (ϕ_2 is the phase difference). $h_r = h_2/h_1$ is the ratio of the harmonics numbers h_1, h_2 in the two rf systems.

For rapid cycling synchrotrons, the V_1, V_2 and ϕ_{1s}, ϕ_{2s} should be synchronized with the rate of change of the dipole magnetic fields with respect to time during beam energy ramping:

$$V_1\sin\phi_{1s} - V_2\sin\phi_{2s} = \rho L\frac{dB(t)}{dt}, \tag{4}$$

where ρ is the bending radius of the dipoles, and L is the circumference of the ring. $B(t)$ is the magnetic field of the dipoles.

The bucket shape in the dual rf system depends on the ratio r of the rf voltage amplitudes in the two harmonic rf systems, defined by $r = V_2/V_1$. When $r > 0.5$, there exist two inner buckets with the two *stable fixed points* (SFPs) in the rf bucket [16]. The positions of the two SFPs (in units of phase) ϕ_{f1} and ϕ_{f2} can be obtained via the minimum of the derivative of the potential

$$\frac{dU_1(\phi)}{d\phi} + \frac{dU_2(\phi)}{d\phi}\bigg|_{\phi=\phi_f} = 0, \tag{5}$$

or more explicitly

$$-r\sin(h_r\phi_f - h_r\phi_{1s} + \phi_{2s}) - r\sin\phi_{2s} + \sin\phi_f + \sin\phi_{1s} = 0. \tag{6}$$

For convenience, in the following, we use ϕ_{f1} to represent the SFP of the inner bucket at the side of the beam head, named as "head SFP" of the head inner bucket, while ϕ_{f2}

denotes the SFP at the side of the beam tail, named as "tail SFP" of the tail inner bucket without loss of generality.

A single particle in the two inner buckets closed to the two SFPs takes a harmonic oscillation:

$$\frac{d^2\Delta\phi}{dt^2} + \omega_s^2\Delta\phi = 0, \tag{7}$$

where $\Delta\phi = \phi - \phi_f$ is the phase difference between the particle considered and the SFP. The synchrotron frequency $\omega_s = \omega_0\nu_s$, with ω_0 the angular revolution frequency and the synchrotron tune

$$\nu_s = \sqrt{\frac{\eta h_1 eV_1}{2\pi\beta_s^2 E_s}[-\cos\phi_f + h_r r\cos(h_r\phi_f - h_r\phi_{1s} + \phi_{2s})]}. \tag{8}$$

Clearly, there are two solutions of Eq. (8), ν_{s1} and ν_{s2} for the two inner buckets.

III. SECOND HARMONIC SYNCHRONOUS PHASE SWEEP

The dependency of U_2 on ϕ_{2s} in the potential function of Eq. (3) indicates the rf bucket, and thus the longitudinal beam distribution can be manipulated by adjusting ϕ_{2s}. In the phase sweep method, a nonzero ϕ_{2s} is set to produce two asymmetrical inner buckets: the area of one inner bucket is increased with enhanced capability of accumulating particles, while the area of the other is decreased.

For an illustrative example, the evolution of the particle distribution in the longitudinal phase space during the multiturn injection based on the parameters in Table I are plotted and shown in Fig. 1, with $\phi_{2s} = 0°$ and 30°, respectively. The code PyORBIT [17] is employed to carry out the PIC simulations with longitudinal space charge. After some modifications [15,18–20], PyORBIT is capable for particle tracking in the dual rf system for rapid cycling synchrotrons.

In the example shown in Fig. 1, the beam is injected into the rf bucket with a minus momentum offset (−0.26%) at $t = 0$. Particles then perform the synchrotron motion clockwise in the phase space (for $\eta > 0$, it is counterclockwise). After a quarter of the synchrotron oscillation period $t = T_s/4$, more particles are accumulated in the tail inner bucket, causing an increased local line density at $t = T_s/4$ and $t = T_s/2$. In comparison, in the presence of a reduced area of the tail inner bucket with $\phi_{2s} = 30°$, particles are distributed more uniformly, hence producing a larger bunching factor.

In the phase sweep method adopted in J-PARC, the variation on ϕ_{2s} is programmed as a linear decrease with time

$$\phi_{2s} = \frac{\phi_{sw}}{T_{inj}}\left(t - \frac{T_{inj}}{2}\right), \tag{9}$$

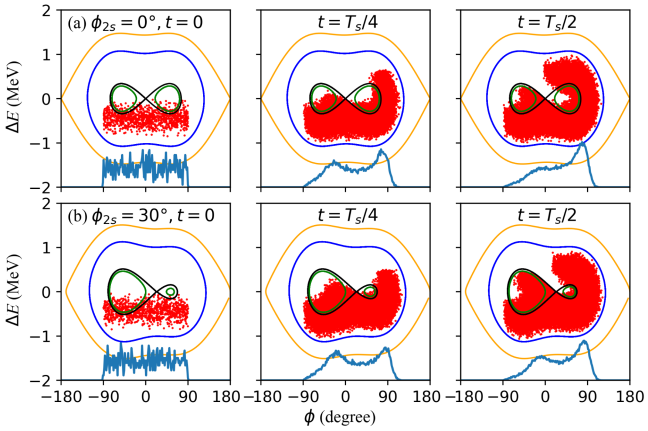

FIG. 1. Snapshots of phase-space distributions of the injected beam at the beginning (left), the first one quarter (middle), and the half (right) of the synchrotron period with $\phi_{2s} = 0°$ (a) and $\phi_{2s} = 30°$ (b). The separatrix of the rf bucket in the dual rf system is shown in orange lines. The blue lines represent the trajectories of the edge particles to guide the eye. The unstable and stable separatrix of the inner buckets are shown in black and green lines, respectively. The projected line densities are shown in blue.

where ϕ_{sw} is the phase sweeping range, T_{inj} is the injection time, and $t \in (-T_{inj}/2, T_{inj}/2)$. The linear phase sweep scheme with Eq. (9) has been successfully applied in the beam injection procedure of the J-PARC RCS [9].

The phase sweep scheme qualitatively described above is obtained mainly based on numerous simulations and experimental attempts. A quantified criterion for the sweeping curve optimization is needed for a *quantitative* understanding of the physical mechanism of beam injection with phase sweeping.

IV. MATCHED PHASE SWEEP SCHEME

The phase sweep method described in Sec. III implies the bunching factor can be improved with a nonzero second harmonics synchronous phase ϕ_{2s}. In order to establish a *quantified* criterion for the bunching factor optimization with ϕ_{2s} during beam injection in the dual harmonic rf system, we propose a "matched phase sweep" scheme, in which the synchrotron oscillation frequency (period) is set to match the beam injection period. The scheme consists of two stages, and the physical mechanism of each stage is detailed analyzed as follows.

A. First stage: Synchrotron frequency maximizing

For convenience, in the following, we take the multiturn painting injection process shown in Fig. 1 as an example.

During the first 1/4 synchrotron period with a nonzero momentum offset, more particles move to and are "trapped" in the tail inner bucket [see the panel (a) and (b) of Fig. 1], causing a large nonuniform particle distribution. In order to reduce the distribution nonuniformity

and thus improve the bunching factor, an initial second harmonics synchronous phase $\phi_{2s,0}$ with the largest synchrotron tune of the head inner bucket $\nu_{2s,max}$ is set to "facilitate" the speed of the synchrotron motion of the particles in the head inner bucket. By doing this, more particles can be "attracted" from the tail inner bucket into the head inner bucket.

The $\nu_{2s,max}$ and the corresponding $\phi_{2s,0}$ can be theoretically computed via Eq. (5) combined with Eq. (8). For rapid cycling synchrotrons, the synchronization relation in Eq. (4) has to be taken into account. Nevertheless, during beam injection in the bottom of the sinusoidal waveform of the energy ramping curve, the slope of the slow ramp is approximately equal to zero. After safely neglecting the acceleration, the combined equation set can be written as

$$\begin{cases} \frac{\partial \nu_s(\phi_{1s},\phi_{2s},\phi_f)}{\partial \phi_{2s}} = 0 \\ \sin\phi_{1s} = r\sin\phi_{2s} \\ \sin\phi_f = r\sin(h_r\phi_f - h_r\phi_{1s} + \phi_{2s}). \end{cases} \tag{10}$$

In practice, $\nu_{2s,max}$ can be obtained numerically. Figure 2 shows the numerical calculation of the variation of synchrotron tunes and the heights of the two inner buckets with respect to ϕ_{2s} using the parameters in Table I, with the fundamental rf voltage amplitude $V_1 = 34$ kV, and the voltage ratio $r = 0.8$ as an example. By inspecting this figure, we find $\nu_{2s,max} = 9.1 \times 10^{-3}$ with $\phi_{2s,0} = 70°$. Furthermore, the inner bucket heights are proportional to the synchrotron tunes. As shown in Fig. 2, when $\nu_{2s} = \nu_{2s,max}$, the head inner bucket has the largest bucket height.

One interesting question may be raised as to if the positions of the stable fixed point of the inner buckets

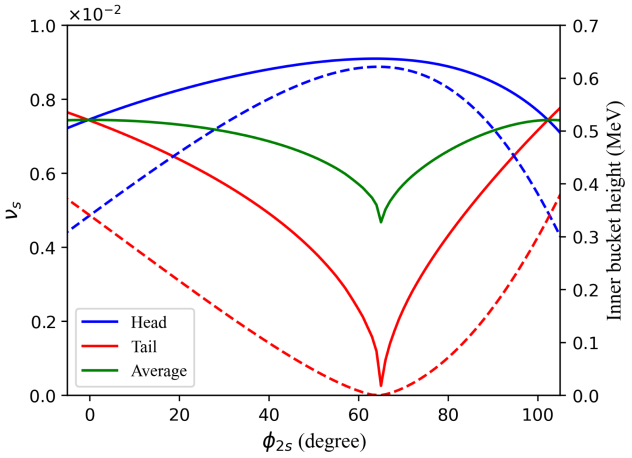

FIG. 2. Left ordinate: Variation of the two synchrotron tunes of the head inner bucket (blue solid), the tail inner bucket (red solid), and their average (green solid), as functions of ϕ_{2s}. Right ordinate: Variation of the heights of the head inner bucket (blue dashed) and the tail inner bucket (red dashed), as functions of ϕ_{2s}.

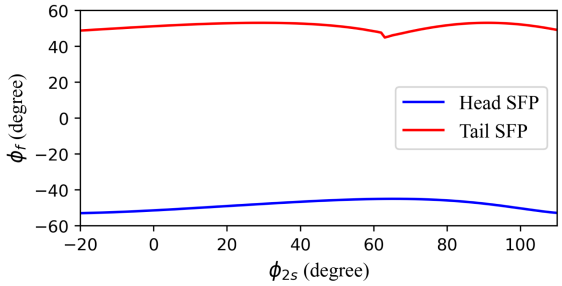

FIG. 3. Variation of the phase positions of the two SFPs in the head inner bucket (red) and in the tail inner bucket (blue) with respect to ϕ_{2s}, as functions of ϕ_{2s} (in the absence of acceleration).

(SFPs) can play a role on the bunching factor optimization, besides the $\nu_{2s,max}$. To address this point, the SFPs as functions of ϕ_{2s} are plotted in Fig. 3. One can see that with varying ϕ_{2s}, the two SFPs are almost constant ($-52.8.0° < \phi_{f1} < -45.0°$ and $44.9° < \phi_{f2} < 53.1°$ in this figure). The SFPs are insensitive to the phase sweeping.

In fact, one can find from Eq. (4) combined with Eq. (5), the bunching factor is determined by ν_{2s}, rather than the SFP (ϕ_f) of the inner bucket. As a result, the change of the synchrotron frequency is proportional to the heights and the areas of the inner bucket and can be taken as a criteria for the ability of accumulating particles. A more illustrative example in Fig. 4 shows the phase-space trajectories with different ϕ_{2s} calculated from Eq. (10). It can be seen that with ϕ_{2s} increasing from 0° to 70°, the area of the head inner bucket is increasing, indicating the enhanced capability of accumulating particles.

The choice of the $\nu_{2s,max}$ employed in the first stage of the matched phase sweep scheme ensures an optimized bunching factor via the increase of the uniformity of the particle distribution in the first 1/4 synchrotron period during injection.

A simulation example is conducted to support the above discussions. In the simulation, the CSNS RCS parameters in Table I are used. The simulation results of the evolution of bunching factors with three typical ϕ_{2s} are presented in Fig. 5. One can see that the bunching factors reach the minimum at $1/4\ T_s$, due to the initial nonzero momentum offset. Since then, the bunching factor with $\phi_{2s} = 70°$ (when $\nu_{2s} = \nu_{2s,max}$) is the largest within 200 turns ($3/4\ T_s$) among the three cases, which is in agreement with the theoretical analysis above.

However, one can observe from Fig. 5 that the bunching factor with $\phi_{2s} = 70°$ starts to decrease and becomes smaller than other two cases at around $3/4\ T_s$. We attribute this to the fact that more particles are trapped in the head inner bucket with $\nu_{2s,max}$ after $3/4\ T_s$. To solve this problem, a matching condition has to be taken into account to achieve a largest bunching factor at the end of the injection, which is discussed in the next subsection.

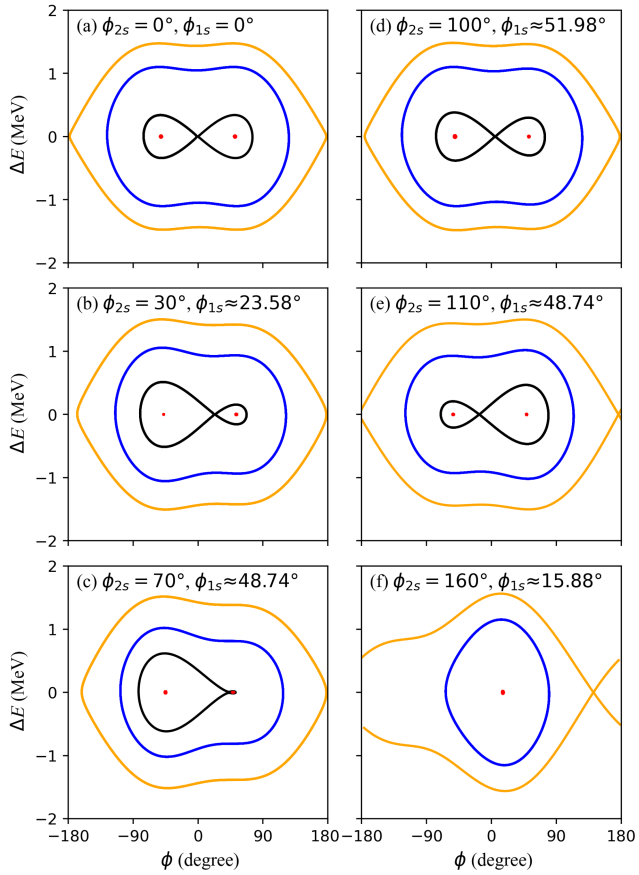

FIG. 4. Phase-space trajectories with six different ϕ_{2s} in the absence of acceleration. (Orange line: Separatrix of the Hamiltonian; blue line: The trajectory with half of the Hamiltonian; black line: Separatrix of the inner bucket; and red dots: The positions of the two SFPs). The synchronous phases in the fundamental rf system ϕ_{1s} are calculated based on the given ϕ_{2s}.

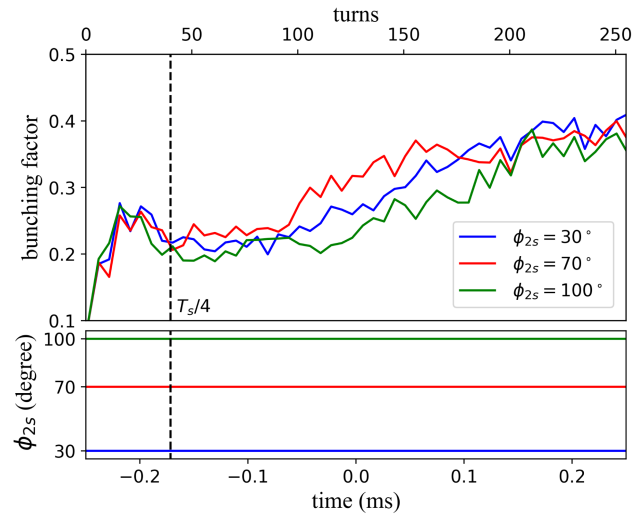

FIG. 5. Comparison of the bunching factor evolution during beam injection with constant $\phi_{2s} = 30°$, 70°, and 100°, respectively.

B. Second stage: Injection period matching

In practice, ν_{2s} is set to zero at the end of the beam injection to produce two symmetrical inner buckets. In order to maximize the bunching factor at the end of beam injection, the second stage of the matched phase sweep scheme is designed as follows.

After keeping $\phi_{2s} = \phi_{2s,0}$ to achieve $\nu_{2s} = \nu_{2s,max}$ in the first stage, ϕ_{2s} was reduced from $\phi_{2s,0}$ to 0 at the end of the beam injection. The $\phi_{2s,0}$ should be decreased in such a way that the integration of the *average value* of the synchrotron tunes ν_{s1} and ν_{s2} of the two inner buckets during the phase sweep is integer multiples of the injection period so that the particles in the two inner buckets can achieve one (or several) average synchrotron period(s) during the injection period, satisfying the matching condition

$$\underbrace{n_0\nu_{s2,max}}_{\text{first stage}} + \underbrace{\int_{n_0}^{n_{inj}} \frac{1}{2}[\nu_{s1}(n) + \nu_{s2}(n)]dn}_{\text{second stage}} = m. \quad (11)$$

Here m is a positive integer. n_0 is the number of the turns during which the maximum synchrotron tune $\nu_{s2,max}$ is set. n_{inj} represents the number of turns for beam injection. With a given set of ($\nu_{2s,max}$, n_{inj}, m), n_0 can be numerically obtained.

The variation curve of ϕ_{2s} for the matched phase sweep scheme can be finally determined based on the two stages discussed above: The initial ϕ_{2s} is set to $\phi_{2s,0}$ until $n = n_{inj}$, and then $\phi_{2s,0}$ is reduced until to zero at the end of the injection.

In order to show the effectiveness of the matching condition with an integer m, an example of the bunching

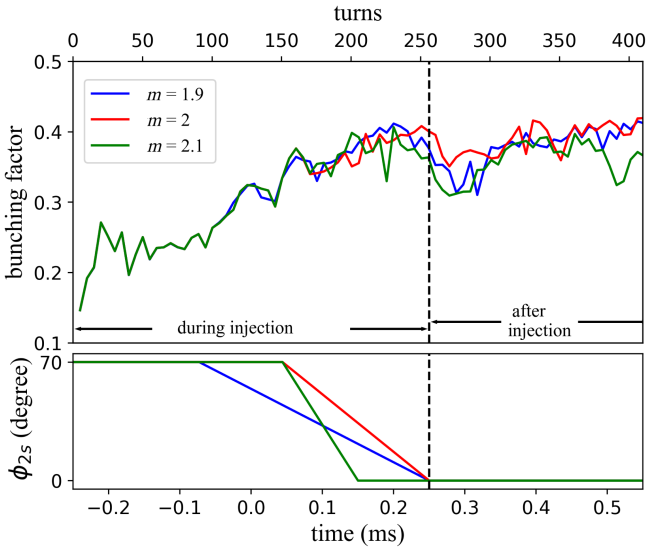

FIG. 6. Comparison of the bunching factor evolution during beam injection with $m = 1.9$, 2.0, and 2.1, respectively.

factor evolution under three different phase sweep scenarios with $m = 1.9$, $m = 2.0$, and $m = 2.1$ calculated from Eq. (11) is given in Fig. 6. It can be seen that during the first half of the injection period, the evolution of the bunching factor is almost the same, since three cases share the same $\phi_{2s,0} = 70°$. However, with the matching condition in Eq. (11) satisfied $m = 2$, the bunching factor after the injection is largest. For $m > 2.0$ or $m < 2.0$, the matching condition is not met. This is a clear support of the matching condition of Eq. (11) for the bunching factor optimization.

V. APPLICATION TO CSNS RCS

The matched phase sweep has been employed successfully for the bunching optimization of the CSNS RCS.

A. PIC simulations

First, PIC simulations are performed to demonstrate the effectiveness of the matched phase sweep scheme. In the simulation, the initial longitudinal beam distribution is randomly uniform in length, and Gaussian in momentum spread, with an injection momentum offset of −0.2% from the designed injection kinetic energy of 80.0 MeV. The initial bunch length is 57 m. The longitudinal space charge calculation is included in the simulation. The number of the macroparticle is 200 000. The multiturn beam injection period takes 255 turns (500 μs). Based on these parameters, the number of turns n_0 for the maximum synchrotron tune frequency $\nu_{2s,max}$ employed in the matched phase sweep is calculated via Eq. (11), obtaining $n_0 = 130$. We thus choose the integer $m = 2$.

The simulations are carried out with four different phase sweep scenarios for comparison: (1) Without phase sweep, $\phi_{2s} = 0°$; (2) with a fixed $\phi_{2s} = 70°$; (3) with a linear sweep of ϕ_{2s}; and (4) with a matched sweep of ϕ_{2s}.

The simulation results of the bunching factor evolution are shown in Fig. 7, which can be divided into three stages: During injection, after injection, and the saturated oscillation. The average value of the bunching factor in each stage is compared in Table II and detailed discussed as follows.

During $t < T_s/4$, a large oscillation of the bunching factors exists due to the momentum offset. As a result, the bunching factor with $\phi_{2s} = 0$ at $t = T_s/4$ is larger than other three cases with $\phi_{2s} \neq 0$.

For $t \geq T_s/4$, the bunching factor with $\phi_{2s} = 0$ becomes smaller than the other three cases with nonzero ϕ_{2s}, since a nonzero ϕ_{2s} can improve the bunching factor in this period. Moreover, compared to the linear case (green color), the bunching factor in the "matched" case (red color) is larger and is overlapped with that in the $\phi_{2s} = 70°$ (orange in Fig. 7), indicating a maximum $\phi_{2s,0}$ helps to improve the bunching factor.

The advantage of the matched phase sweep becomes more apparent after injection. Compared to the "linear" case and the $\phi_{2s} = 70°$ case, the bunching factor with the matched phase sweep scenario is the largest, since the synchrotron frequency is set to match with the injection period.

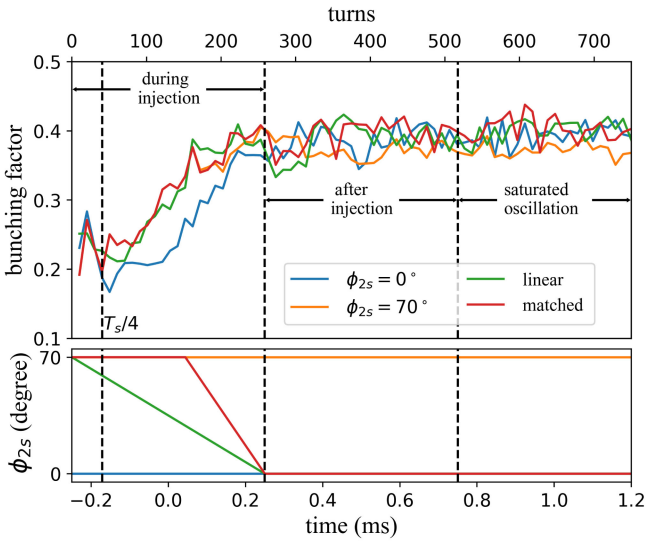

FIG. 7. Simulation results of the bunching factor evolution with four different phase sweep scenarios in the dual rf harmonic system of the CSNS RCS.

This advantage can be also found in the stage of the saturated oscillation. Here, the "saturated" is defined based on the stable evolution of the bunching factor with $\phi_{2s} = 0°$; bunching factors with its standard deviation less than 0.015 refer to be stable.

The average bunching factors during and after injection are listed in Fig. 7. Compared to the case without phase sweep ($\phi_{2s} = 0°$), the average bunching factor is increased by 4.6% with the linear phase sweeping and by 6.0% with the matched phase sweeping.

B. Experimental measurement

Experiments on the bunching factor measurement in the CSNS RCS are conducted to test the matched phase sweep method. In the measurement, the beams are injected into the RCS by using four different phase sweep methods for comparison. The longitudinal profiles of the bunched beams are recorded via the wall current monitor with a sampling rate of 20 MHz. The bunching factor is then

TABLE II. Average value of the bunching factor of the four different scenarios in each stage.

Scenario	During injection	After injection	Saturated oscillation	Difference (%)
$\phi_{2s} = 0°$	0.264	0.386	0.394	⋯
$\phi_{2s} = 70°$	0.305	0.373	0.371	0.5
Linear	0.301	0.379	0.396	4.6
Matched	0.308	0.394	0.403	6.0

TABLE III. Beam parameters used in the experiments.

Parameters (unit)	Value
Injection kinetic energy (MeV)	80.0
Synchronous kinetic energy (MeV)	80.3
Injection turns	255
Injection time duration (ms)	0.5
Injection kinetic energy spread (%)	±0.05
Number of particles per bunch	1.09×10^{13}
Chopper duty	0.5

computed by the ratio of the peak beam current to the average beam current. Main beam parameters used in the experiment are summarized in Table III.

First, the measurement is performed in the absence of beam acceleration. The measurement results of the bunch profiles with four different phase sweep methods during injection (at 55th turns) are shown in Fig. 8. Compared to the other two scenarios (i.e., the $\phi_{2s} = 0°$ case and the linear case), the peak current of the bunch is much reduced with the matched phase sweep method. Note that the beam profile with the matched phase sweep and with the $\phi_{2s} = 70°$ case are overlapped in the injection period in Fig. 8, which is in agreement with the simulation results in Fig. 7, indicating the maximum synchrotron tune $\nu_{2s,max}$ with the corresponding $\phi_{2s} = 70°$ has an obvious effect on reducing the peak current during beam injection.

The measurement results of the bunch profiles after injection (at 1000th turns) are shown in Fig. 9. One can observe that the bunch profile under the matched phase sweep method becomes more uniform than the other three cases.

Figure 10 shows the measurement results of the bunching factor evolution during and after injection. Compared to other three cases, the bunching factor with the matched phase sweep method is much improved.

To check the reproducibility of the measurement results of the bunching factor shown in Fig. 10, additional measurements with $V_1 = 20$ kV and $V_2 = 16$ kV are conducted. The experimental results of 10 times of the repeated measurement on the bunching factor are shown in Fig. 11. It can be seen that compared to the linear phase sweep case, the bunching factor becomes larger with the adoption of the matched phase sweep method.

Second, the measurement in the presence of beam acceleration is performed. Beams are injected and accelerated in the RCS within 20 ms and then extracted. The beam parameters are the same as summarized in Table III.

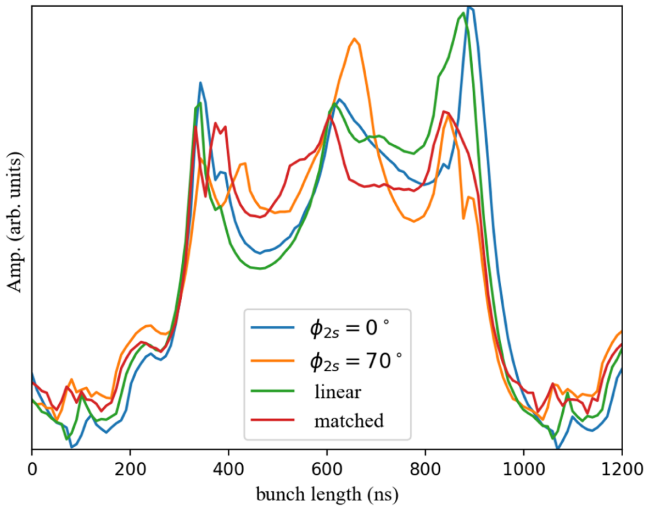

FIG. 9. Measurement results of the bunch profile after injection at 800 turns (1.315 ms) with four different phase sweep scenarios in the absence of acceleration.

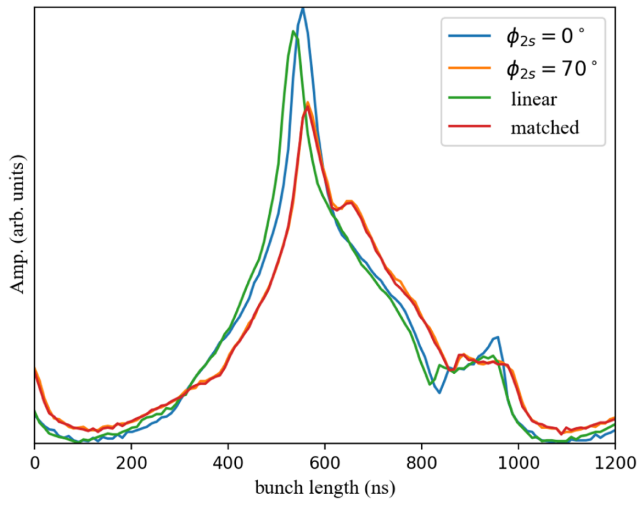

FIG. 8. Measurement results of the bunch profile during injection at 55 turns (−0.142 ms) with four different phase sweep scenarios in the absence of acceleration.

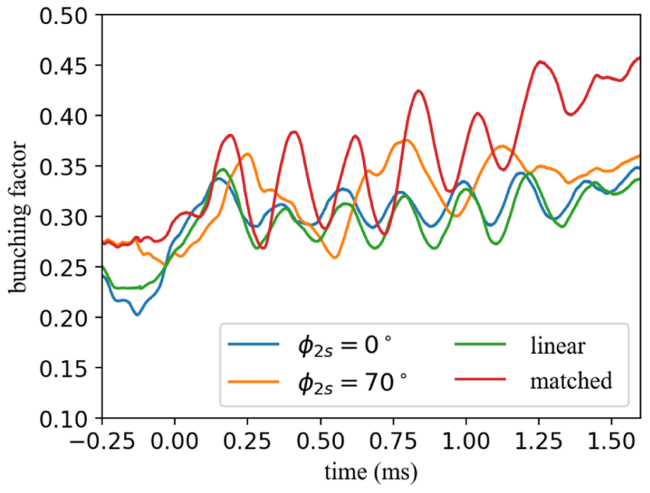

FIG. 10. Measurement results of the bunching factor with four different phase sweep scenarios in the CSNS RCS. The beam injection starts at −0.25 ms.

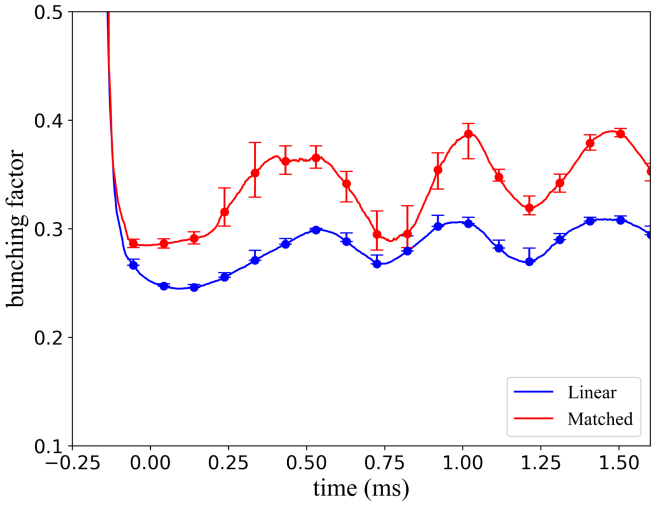

FIG. 11. Repeated measurement results of the bunching factor with the linear phase sweep method and the matched phase sweep method in the CSNS RCS.

The measurement results and the rf voltage waveform used in the experiment are, respectively, shown in the top and the bottom panel of Fig. 12. Compared to the linear sweep case, the bunching factor with the matched phase sweeping is much increased.

It is worth pointing out that the measured bunch profiles with the different phase sweep methods in Figs. 9 and 13 have almost the same bunch length. The larger bunching factor with the matched phase sweeping is because of a more smooth (uniform) density of the bunched beam.

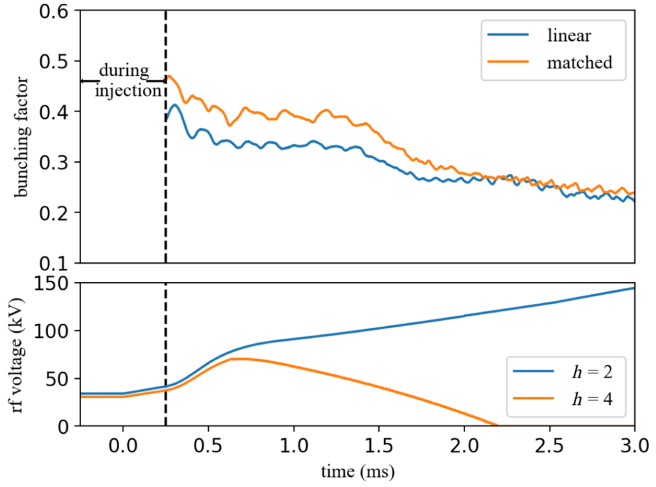

FIG. 12. Top panel: measurement results of the bunching factor after injection with and without matched phase sweep method in the presence of acceleration in the CSNS RCS. Measurement starts at 0.25 ms because of hardware settings [21]. Bottom panel: rf voltage waveform of the dual rf system employed in the measurement.

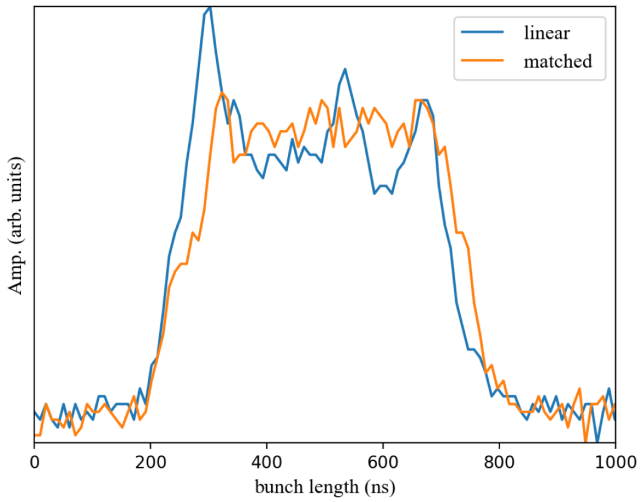

FIG. 13. Measurement results of the bunch profiles after injection at 800 turns (1.3 ms) with and without phase sweep in the presence of acceleration.

VI. GENERAL CASES

The measurement results of the bunching factor in Figs. 10 and 11 show the advantage of the matched phase sweep method for different scenarios in the application on the CSNS RCS. For more general cases, the advantage of the matched phase sweep scheme can become more obvious. To illustrate this, we adjust the voltage amplitude V_2 from 34 to 61.5 kV by keeping $r = 0.8$ with the parameters of the CSNS RCS in Table I. With these parameters, simulations of the beam injection are carried out with the matched phase sweep method, compared with the linear phase sweep scheme, as shown in Fig. 14. For the matched phase sweep method, we obtain $m = 3$ computed from Eq. (11).

One can observe that the bunching factor with the adoption of the matched phase sweep is much larger than that with the linear phase sweep scheme: 10% increase of bunching factor during the injection and 10% increase within 1 ms. Compared to the case in Fig. 7 with $m = 2$, the advantage of the matched phase sweep method in the example with $m = 3$ in Fig. 14 becomes more obvious.

We here introduce a parameter of "normalized average bunching factor difference" ΔBF defined by

$$\Delta\mathrm{BF} = \left\langle \frac{\mathrm{BF}_{\mathrm{matched}} - \mathrm{BF}_{\mathrm{linear}}}{\mathrm{BF}_{\mathrm{linear}}} \right\rangle_{300\ \mathrm{turns}} \tag{12}$$

to compare the average value of the bunching factor from −0.25 ms until 0.34 ms (during 300 turns) obtained with the matched phase sweeping ($\mathrm{BF}_{\mathrm{matched}}$) and with the linear phase sweeping ($\mathrm{BF}_{\mathrm{linear}}$). Here the symbol "$\langle \ldots \rangle$" denotes the average value. For the case in Fig. 14, we obtain $\Delta\mathrm{BF} = 4.11\%$.

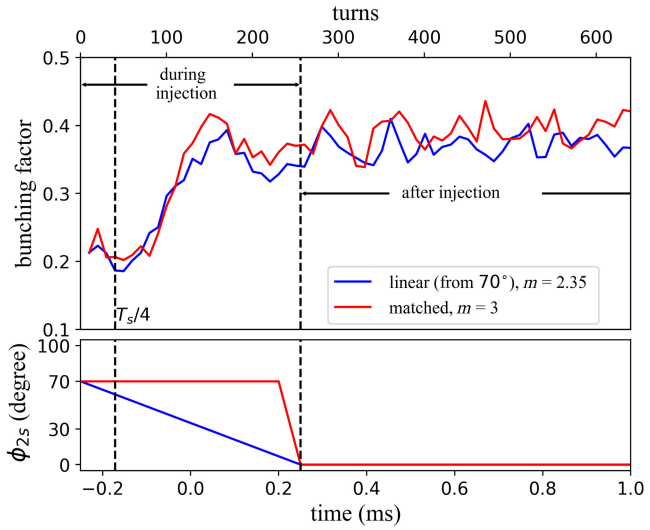

FIG. 14. Simulation results of the bunching factor evolution with the linear phase sweep scheme (blue) and the matched phase sweep scheme (red).

A general scan of ΔBF for comparison of the two phase sweep schemes are obtained via varying V_1 and V_2 and keeping $r = 0.8$ and presented in Fig. 15. The examples in Figs. 7 and 14 are included in this scan (marked as black dots).

One can observe from Fig. 15 with m far away from an integer (1, 2, or 3), ΔBF is increasing, and the merit of the matched phase sweep becomes more obvious. This is because the matching condition in the linear phase sweep scheme is missing with a noninteger m. In other words, when m approaching to an integer 1, 2, or 3, the matching condition is more satisfied, and ΔBF becomes smaller.

Moreover, it is worth pointing out that the matching condition can be satisfied not only via adjusting the voltage amplitudes. In fact, with a suitable choice of longitudinal parameters, such as η, h_1, or E_s in Eq. (8), the linear phase sweep method can also meet the matching condition. In such cases, for an integer m, the two schemes are in agreement with each other.

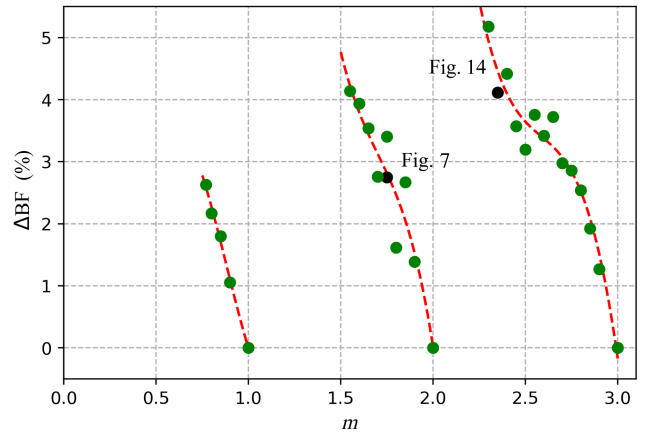

FIG. 15. Scan of the difference on the bunching factors by using the two injection schemes, as a function of m. The red dashed lines are the guide to the eye. The CSNS RCS case in Fig. 7 is marked as blue.

VII. CONCLUSION

In this paper, we have proposed a new phase sweep scheme, namely the matched phase sweep scheme, for the bunching factor optimization during multiturn painting injection in a dual harmonic rf system for high-intensity synchrotrons. The physical mechanism of the phase sweep method is quantitatively detailed descried. Based on the calculation of the largest synchrotron tune of the inner bucket and matched to the injection period, an optimized phase sweep curve can be quantitatively figured out. Compared to the qualitative linear phase sweep method, it is shown in both simulations and machine study in the CSNS RCS that the bunching factor can be increased with the adoption of the matched phase sweep method.

Furthermore, we have shown that the linear phase sweep method is a specific cases of the proposed matched phase sweep method. For some special cases, the optimization effectiveness of the bunching factor based on the two methods is almost in agreement with each other. In more general cases, the merit of the matched phase sweep method is obvious. The matched phase sweep method has been successfully adopted in the routine beam operation of the CSNS RCS and could be also applied to other high-intensity hadron synchrotorns.

ACKNOWLEDGMENTS

The authors would like to thank the CSNS colleagues for the beam commissioning and hardware maintenance. The authors also would like to express their gratitude to Andrei Shishlo on his useful advice on the use of PyORBIT. This work is supported by the Guangdong Basic and Applied Basic Research Foundation (Project No. 2024A1515012658) and the International Partnership Program of Chinese Academy of Sciences (Project No. 013GJHZ2023026FN).

[1] L. J. Laslett, On intensity limitations imposed by transverse space-charge effects in circular particle accelerators, eConf **C630610**, 324 (1963), https://lss.fnal.gov/conf/C630610/p324.pdf.

[2] S. Myers and O. Bruning, *Challenges and Goals for Accelerators in the XXI Century* (World Scientific, Singapore, 2016).

[3] A. Hofmann and F. Pedersen, Bunches with local elliptic energy distributions, IEEE Trans. Nucl. Sci. **26**, 3526 (1979).

[4] D. J. Adams, C. W. Appelbee, D. Bayley, N. Farthing, I. Gardner, M. G. Glover, B. G. Pine, A. Seville, J. Thomason, and C. M. Warsop, Progress on dual harmonic acceleration on the ISIS synchrotron, in *Proceedings of the*

22nd Particle Accelerator Conference, PAC-2007, Albuquerque, NM(IEEE, New York, 2007), p. 1649.

[5] A. Seville, D. Adams, D. Bayley, R. Bendall, I. Gardner, M. Glover, A. Morris, J. Thomason, and C. Warsop, First results from the use of dual harmonic acceleration on the ISIS synchrotron, in *Proceedings of the 21st Particle Accelerator Conference, Knoxville, TN, 2005* (IEEE, Piscataway, NJ, 2005), pp. 1871–1873.

[6] M. Blaskiewicz, J. M. Brennan, and J. Brodowski, Ring rf and longitudinal dynamics in the SNS, in *Proceedings of the 7th European Particle Accelerator Conference, Vienna, Austria, 2000* (2000), https://accelconf.web.cern.ch/e00/PAPERS/TUP3B03.pdf.

[7] D. Quartullo, S. Albright, E. Shaposhnikova, and H. Timko, CERN PS booster longitudinal dynamics simulations for the post-LS2 scenario, in *Proceedings of the 57th ICFA Advanced Beam Dynamics Workshop on High-Intensity and High-Brightness Hadron Beams, ICFA HB-2016, Malmö, Sweden*, (CERN, Geneva, Switzerland, 2016).

[8] M. Yamamoto, M. Nomura, A. Schnase, T. Shimada, H. Suzuki, F. Tamura, E. Ezura, K. Hara, K. Hasegawa, C. Ohmori, K. Takata, A. Takagi, M. Toda, and M. Yoshii, Simulation of longitudinal beam manipulation during multi-turn injection in J-PARC RCS, Nucl. Instrum. Methods Phys. Res., Sect. A **621**, 15 (2010).

[9] F. Tamura, M. Yamamoto, M. Yoshii, C. Ohmori, M. Nomura, A. Schnase, M. Toda, H. Suzuki, T. Shimada, K. Hara, and K. Hasegawa, Longitudinal painting with large amplitude second harmonic rf voltages in the rapid cycling synchrotron of the Japan Proton Accelerator Research Complex, Phys. Rev. ST Accel. Beams **12**, 041001 (2009).

[10] J. Wei, H. S. Chen, Y. W. Chen *et al.*, China Spallation Neutron Source: Design, R&D, and outlook, Nucl. Instrum. Methods Phys. Res., Sect. A **600**, 10 (2009).

[11] S. Wang, S. X. Fang, S. N. Fu, W. B. Liu, H. F. OuYang, Q. Qin, J. Y. Tang, and J. Wei, Introduction to the overall physics design of CSNS accelerators, Chin. Phys. C **33**, 1 (2009).

[12] S. Xu, H. Liu, J. Peng, J. Chen, L. Huang, M. Huang, M. Li, X. Lu, X. Luo, and Y. Li, Beam commissioning and beam loss control for CSNS accelerators, J. Instrum. **15**, P07023 (2020).

[13] J. Peng, CSNS-II superconducting Linac design, in *Proceedings of the 31st Linear Accelerator Conference, LINAC-2022, Liverpool, UK* (JACoW, Geneva, Switzerland, 2022).

[14] Y. S. Yuan, N. Wang, S. Y. Xu, Y. Yuan, and S. Wang, Theoretical study of a dual harmonic system and its application to the CSNS/RCS, Chin. Phys. C **39**, 127002 (2015).

[15] H. Liu and S. Wang, Longitudinal beam dynamic design of 500 kW beam power upgrade for CSNS-II RCS, Radiat. Detect. Technol. Methods, **6**, 339 (2022).

[16] S. Y. Lee, *Accelerator Physics*, 3rd ed. (World Scientific, Singapore, 2011).

[17] A. Shishlo, S. Cousineau, J. Holmes, and T. Gorlov, The particle accelerator simulation code PyORBIT, Proc. Comput. Sci. **51**, 1272 (2015).

[18] Y.-S. Yuan, N. Wang, S.-Y. Xu, and S. Wang, A code for the optimization of rf voltage waveform and longitudinal beam dynamics simulation in an RCS, Nucl. Instrum. Methods Phys. Res., Sect. A **729**, 864 (2013).

[19] L. Huang, H. Liu, M. Li, S. Xu, Y. An, Z. Li, Y. Li, M. Huang, Y. Yuan, and J. Peng, Longitudinal dynamics study and optimization in the beam commissioning of the rapid cycling synchrotron in the China Spallation Neutron Source, Nucl. Instrum. Methods Phys. Res., Sect. A **998**, 165204 (2021).

[20] H. Liu, X. Lu, S. Xu, L. Huang, X. Feng, M. Li, and S. Wang, Beam dynamics simulation about the dual harmonic system by PyORBIT, in *Proceedings of the 12th International Particle Accellarator Conference, IPAC-2021, Campinas, SP, Brazil* (JACoW, Geneva, Switzerland, 2021).

[21] CSNS Beam Diagnostic Group (private communication).